PHILOSOPHICAL MAGAZINE LETTERS, 2017
http://dx.doi.org/10.1080/09500839.2017.1316019

Taylor & Francis
Taylor & Francis Group

Check for updates

Plastic deformation of B2-NiTi – is it slip or twinning?

H. Sehitoglu, Y. Wu, S. Alkan and E. Ertekin

Department of Mechanical Science and Engineering, University of Illinois at Urbana-Champaign, Urbana, IL, USA

ABSTRACT
The work addresses two main questions that have baffled the shape memory research community. Firstly, the superb ductility of B2-NiTi cannot be solely attributed to slip on {0 1 1} planes, because there are not a sufficient number of independent slip systems under arbitrary deformations. We show unequivocally, upon diffraction measurements and local strain field traces, that deformation twinning on {1 1 4} planes that can provide additional systems to accommodate plastic flow is activated. Secondly, the slip direction on the {0 1 1} planes has not been established in NiTi with certainty. It is proved precisely to be in ⟨0 0 1⟩ direction based on crystallographic shear analysis producing the specific strain tensor components (measured at mesoscale with digital image correlation, DIC). Based on the single-crystal experiments, the CRSSs (critical resolved shear stress) are established as 250 and 330 MPa for slip and twinning, respectively. The results have implications in devising correct crystal plasticity formulations for shape memory alloys.

ARTICLE HISTORY
Received 1 February 2017
Accepted 27 March 2017

KEYWORDS
Deformation twinning; slip bands; Ni-Ti alloys; EBSD; shape memory alloys; plastic deformation; dislocations; twinning; {1 1 0}⟨0 0 1⟩ slip; {1 1 4} twinning; B2 austenite

1. Introduction

The NiTi remains the most remarkable shape memory alloy (SMA) whose transformation response has been well-studied while its plastic flow behaviour is far less understood [1–12]. The plastic flow has been linked to an increase in thermal and stress hysteresis [3,7] via increased dissipation, a lowering of transformation strains [1,4,6,13] instigated by accumulation of inelastic strains at high applied stresses, the increase in strain hardening response [14,15] via dislocation interactions thereby limiting reversibility, a lowering of fatigue resistance [16,17] by increasing irreversibility at crack tips and a decrease in elastocaloric cooling capacity upon cycling [18,19]. Because of the prominence of plastic deformation, the topic is receiving more attention recently [12,20,21], including reviews [22]. Plastic deformation of austenite can readily occur at austenite–martensite interfaces [9,10,23] and also in untransformed austenite domains depending on the deformation temperature [24].

The plastic deformation properties can be readily assessed based on tension or compression experiments above M_d [5,25,26], the temperature above which the austenite (B2)

CONTACT H. Sehitoglu huseyin@illinois.edu

© 2017 Informa UK Limited, trading as Taylor & Francis Group

deforms elastoplastically. There are two main questions regarding the plastic deformation: (i) if it occurs via *slip* what is the prevailing slip system (plane and direction)?, (ii) if *deformation twinning* occurs, what is the prevailing twin system? To address these questions, we undertake an experimental deformation study of single crystal specimens of four selected orientations to assess the propensity for slip and twinning by examining the surface strain traces of all plausible systems. The elastic homogeneity associated with single crystals leads to a clear translation from microscopic shear to macroscopic strain tensors. In summary, a combination of digital image correlation (DIC) observations of strain localisation, electron backscattering diffraction results and crystalline plasticity relations were utilised to reveal the onset of specific twinning and slip systems.

2. Slip and twin systems in NiTi alloy

Several slip systems have been forwarded for NiTi alloys [5,12]. The three potential slip systems are the following: $\{0\ 1\ 1\}\langle 0\ 0\ 1\rangle$, $\{0\ 1\ 1\}\langle 1\ 1\ 1\rangle$, and $\{0\ 0\ 1\}\langle 1\ 0\ 0\rangle$. Based on energetic grounds [12], the $\{0\ 1\ 1\}\langle 0\ 0\ 1\rangle$ slip system has the lowest energy barrier (the unstable peak value) of 142 mJ m^{-2} and hence is most likely to be activated. There are six physically possible (or geometric) slip systems for this case. However, only three out of the six physically possible ones are independent [12]. Therefore, the $\{0\ 1\ 1\}\langle 0\ 0\ 1\rangle$ system cannot produce five independent slip systems to satisfy the Mises criteria [27] for arbitrary deformations. The $\{0\ 1\ 1\}\langle 1\ 1\ 1\rangle$ is a harder slip system and can be activated at high stress levels to produce five independent slip systems [12] (out of physically possible 12 slip systems). Finally, the $\{0\ 0\ 1\}\langle 1\ 0\ 0\rangle$ is the hardest slip system to activate, and cannot produce five independent slip systems. It has hardly been observed. The question is whether $\{0\ 1\ 1\}\langle 0\ 0\ 1\rangle$, $\{0\ 1\ 1\}\langle 1\ 1\ 1\rangle$, or both are most likely to activate under deformation? To answer this question, we forward a resourceful method utilising single crystals in conjunction with the strain field measurements arising from these two systems, respectively, to pinpoint the active system. These two slip systems produce drastically different crystallographic strain tensors, respectively, at the specimen coordinate frame. Based on our results, we rule out the $\{0\ 1\ 1\}\langle 1\ 1\ 1\rangle$ slip and establish $\{0\ 1\ 1\}\langle 0\ 0\ 1\rangle$ as the dominant slip system.

For twinning, two twin systems have been proposed for NiTi binary alloys: $\{1\ 1\ 4\}$ mechanical twins and $\{1\ 1\ 2\}$ pseudo-twins [28,29]. Both $\{1\ 1\ 4\}$ and $\{1\ 1\ 2\}$ twinning can produce the five independent twin systems [30]. In this paper, we also address whether $\{1\ 1\ 4\}$ twinning or $\{1\ 1\ 2\}$ pseudo-twinning is activated? Energetically, the $\{1\ 1\ 4\}$ twin is more favourable but this does not rule out the possibility of a $\{1\ 1\ 2\}$ twin [29]. In this study, by matching the projections of the twin planes on the sample surface with the observed traces associated with the localised strains measured via DIC, one can determine the twin planes unequivocally. The results show activation of $\{1\ 1\ 4\}$ twinning. This is corroborated with Electron Back Scatter Diffraction (EBSD) measurements.

3. The NiTi alloy and experimental results

To gain insight into plastic deformation in NiTi, we need to use single crystals where the planes and directions are well defined. After growth of NiTi using the Bridgman method, the crystals were subjected to homogenisation at 1000 °C for 20 hrs and solutionising at 930 °C for 30 min followed by water quench. The single crystals selected for this study were

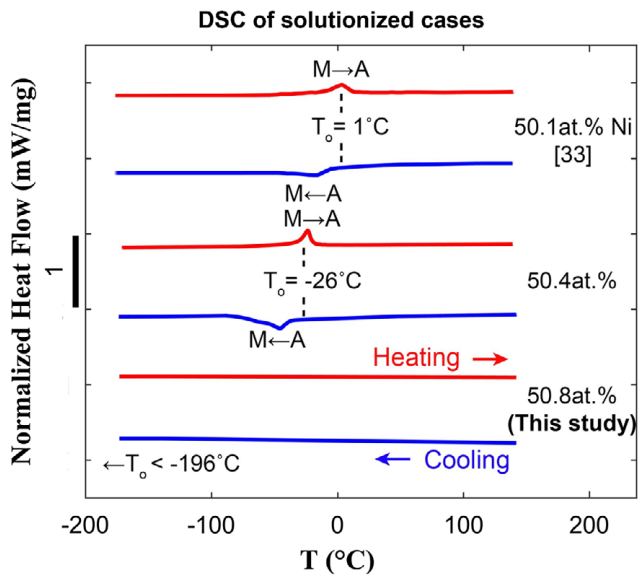

Figure 1. Normalised DSC curves of the NiTi alloys with 50.1 [33], 50.4 and 50.8 at.% Ni content in the solutionised condition. Amongst all, we study the NiTi alloys with 50.8 at.% Ni in the solutionised condition at room temperature. *A* is the austenite, *M* represents martensite, and T_o is the equilibrium temperature.

Table 1. Euler's angles obtained from EBSD(+ denotes orientation of twinned domain).

Loading direction [*l m n*]	[0 1 0]	[0 1 0] twin+	[$\bar{9}$ 2 4]	[$\bar{1}$ 0 1]	[1 1 $\bar{1}$]
φ_1	18°	69°	135.2°	113.1°	64.7°
Φ	9.7°	39°	33.4°	47.7°	40.8°
φ_2	72°	83°	53.1°	64.2°	84.8°

Ni rich with a composition of 50.8 at.% Ni. The differential scanning calorimeter (DSC) results of the solutionised NiTi alloys with 50.1, 50.4 and 50.8 at.% Ni are illustrated in Figure 1, where A is the cubic austenite (B2) and M represents the monoclinic martensite (B19′). The DSC scan was performed at a rate of 10 °C/min within a temperature range from −196 to 140 °C. In Figure 1, the single-step phase transformation between B2 and B19′ was observed, which is also typical of the solutionised near equi-atomic NiTi [31–33]. A two-stage transformation (with an intermediate R-phase formation) is ubiquitous upon ageing treatments [33], at high Ni contents [34], and with the addition of ternary elements [35]. In Figure 1, the equilibrium temperature, T_o, approximated by $\frac{1}{2}\left(M_s + A_f\right)$ [36], is marked to indicate the shift of transformation temperatures as the Ni content increases. It is evident that the T_o decreases with increasing Ni content (from 50.1 [33] to 50.4 at.%) and drops dramatically at 50.8 at.% Ni and higher Ni contents [34]. At 50.8 at.% Ni, the T_o is well below −196 °C (77 K), which is too low to be detected by the DSC technique. Since the deformation at room temperature (25 °C) is significantly above the transformation temperatures, the deformation occurs via slip and no phase transformation is expected. This fact is confirmed upon EBSD measurements on deformed samples where either slip or deformation twinning has taken place.

We have conducted uniaxial tensile and compressive experiments on single crystals with their loading axis aligned with [0 1 0], [$\bar{1}$ 0 1], [1 1 $\bar{1}$], and [$\bar{9}$ 2 4] crystal orientations. These crystallographic orientations have been verified by the Euler's angles procured via EBSD in

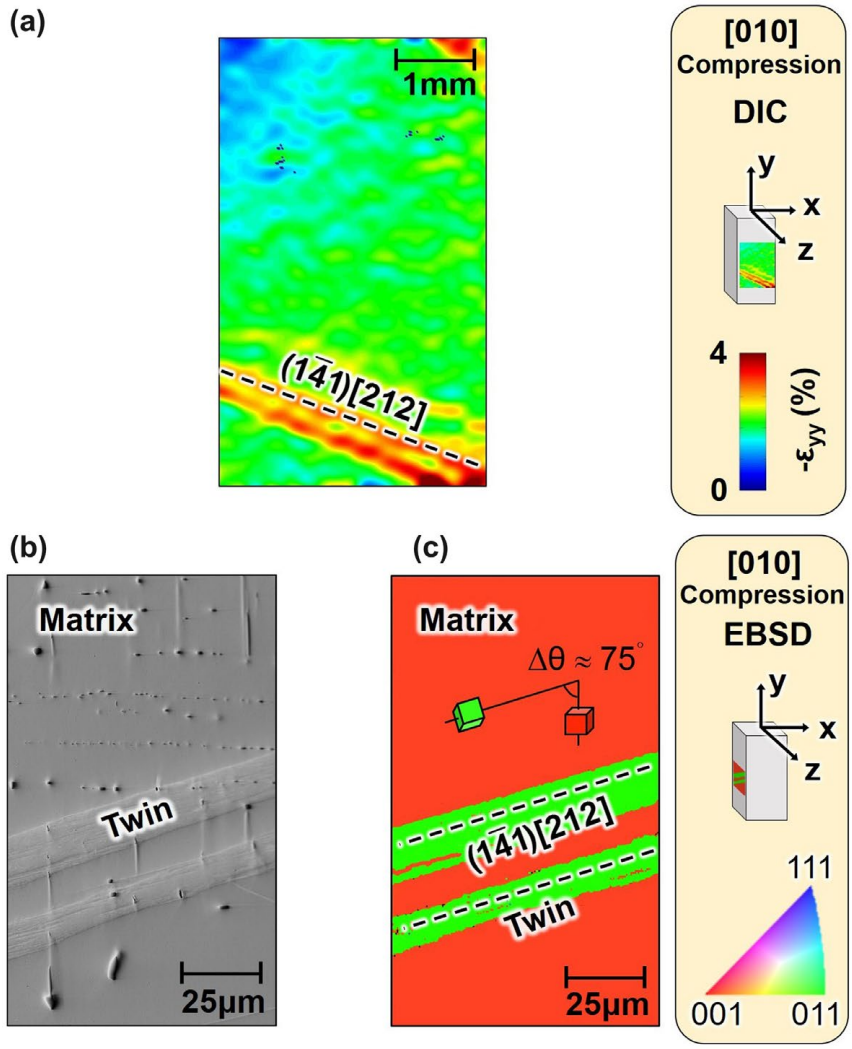

Figure 2. (a) The front surface of the specimen showing the local DIC strain field associated with twinning. Note that a single system is activated (details are given in the text). The activation of twinning in [0 1 0] compression case is proved in (b) and (c). The left side surface of the compression specimen shows the (b) SEM micrograph and (c) the EBSD pattern indicating the twin bands.

the Bunge convention [φ_1, Φ, φ_2] (Table 1). To determine the loading direction, for example, the Euler's angles representation can be converted to the corresponding Miller indices [$l\,m\,n$], which has been expressed in Equation (1) [37,38]. We will discuss the [0 1 0] case first followed by the [$\bar{9}$ 2 4] case showing the DIC-based strain fields. Then, we elaborate on the [$\bar{1}$ 0 1] and [1 1 $\bar{1}$] case in the discussion section.

$$\begin{bmatrix} l \\ m \\ n \end{bmatrix} = \begin{bmatrix} \cos\varphi_1 \cos\varphi_2 - sin\varphi_1 \sin\varphi_2 \cos\Phi \\ -\cos\varphi_1 \sin\varphi_2 - \sin\varphi_1 \cos\varphi_2 \cos\Phi \\ \sin\varphi_1 \sin\Phi \end{bmatrix} \tag{1}$$

3.1. Twinning- the [0 1 0] compression loading case

We first consider the case of [0 1 0] single crystal subjected to compression. The sample has a square cross-section and all the normal orientations are also known with EBSD

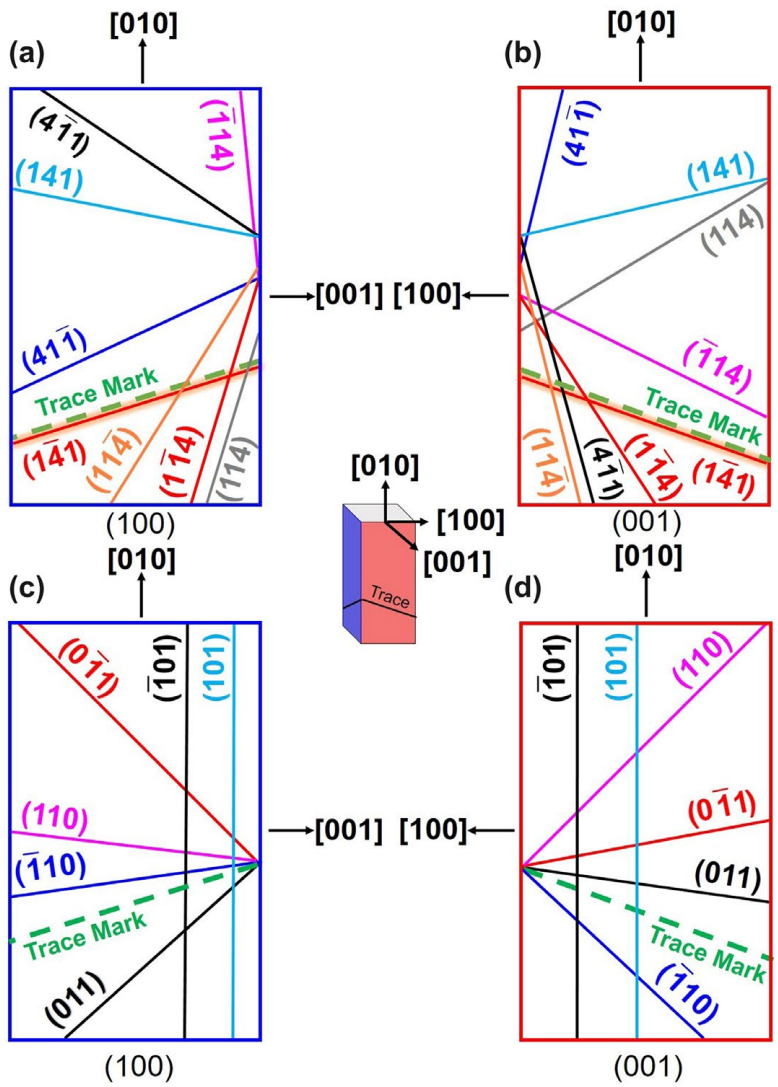

Figure 3. (a) The projections of the {1 1 4} twin plane family on the left side surface and (b) the front surface. The measured trace is marked on both surfaces with the 'green' line. It coincides with the (1 $\bar{4}$ 1) plane. The traces of the {0 1 1} planes on (c) the side and (d) front surface of the specimen. The results show that the trace mark does not coincide with any of the {0 1 1} slip systems.

measurements. The localised strains are shown in Figure 2a on the front surface to demonstrate the localisation of plastic deformation. The trace of the same bands on the side surface is depicted via SEM micrograph in Figure 2b. These localised bands are associated with the activation of a particular slip or twin system. To precisely identify the observed strain bands, EBSD was undertaken on the left side surface and the results are illustrated in Figure 2c. The misorientation of the twin region with respect to the loading axis is determined as 75° using Equations (2) and (3), where g is the orientation matrix [37] that depends on the Euler angles measured from EBSD (Table 1). This angle corresponds precisely to the twin-matrix misorientation between {0 0 1} and {1 1 4} planes.

$$\Delta g = g_{\text{matrix}} \cdot g_{\text{twin}}^{-1} \tag{2}$$

$$\theta = \arccos\left(\frac{\text{trace}(\Delta g) - 1}{2}\right) \tag{3}$$

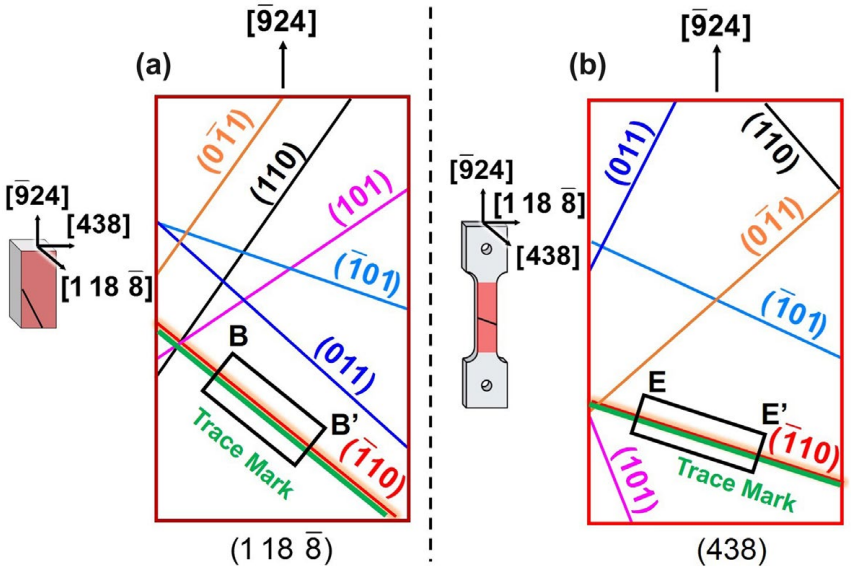

Figure 4. The traces of the {0 1 1} planes on the front surface of the specimen for compression (a) and tension (b). The results show that the trace mark coincides with the projection of ($\bar{1}$ 1 0) plane marked with BB′ and EE′.

The trace of the deformation plane is depicted schematically in Figure 3. The front surface is the DIC plane, whilst the left side surface represents the photographed surface. Now, we set out to determine the orientation of this localisation plane by superimposing the potential slip {0 1 1} and twin {1 1 4} traces at the macroscale.

In Figures 3a and b, the projections of the {1 1 4} twin systems onto the front and side surfaces of the crystal are shown. The trace mark measured experimentally is superimposed in both Figures 3a and b as well. It is clear that the observed trace corresponds to the projection of (1 $\bar{4}$ 1) plane in this case. In Figures 3c and d, the traces of six {0 1 1} slip systems are shown, and we note that the {0 1 1} plane does not correspond to the 'localisation' trace.

In summary, the results show unequivocally that {0 1 1} slip cannot be active in the [0 1 0] single crystal compression case. In fact, the (1 $\bar{4}$ 1) plane, which belongs to the twin family in NiTi, is activated in this case. The CRSS for twinning in this case is determined as 330 MPa using a Schmid factor of 0.354. This twin system can provide additional systems to accommodate the large degree of plastic flow observed in NiTi.

3.2. *Crystallographic slip – the [$\bar{9}$ 2 4] tension and compression loading case*

We now investigate the three orientations that exhibit plastic deformation via slip. In three of the orientations, [$\bar{1}$ 0 1], [$\bar{9}$ 2 4], and [1 1 $\bar{1}$], tested in this study, the slip plane is determined as {0 1 1}. The slip trace analysis was shown for the [$\bar{9}$ 2 4] case in Figure 4. The slip plane was identified as the ($\bar{1}$ 1 0) plane marked with BB′ and EE′ for compression and tension, respectively. In Figure 5, we present the corresponding strain components (ε_{yy}, ε_{yy} and ε_{xy}) produced by the slip shear on the same ($\bar{1}$ 1 0) plane (BB′ and EE′) shown for the [$\bar{9}$ 2 4] case.

The determination of the slip direction requires an additional step because on the {0 1 1} plane the slip direction can be ⟨0 0 1⟩ or ⟨1 1 1⟩. We propose and use a novel method to distinguish between ⟨0 0 1⟩ or ⟨1 1 1⟩ slip as explained next. As a first step, we calculated the

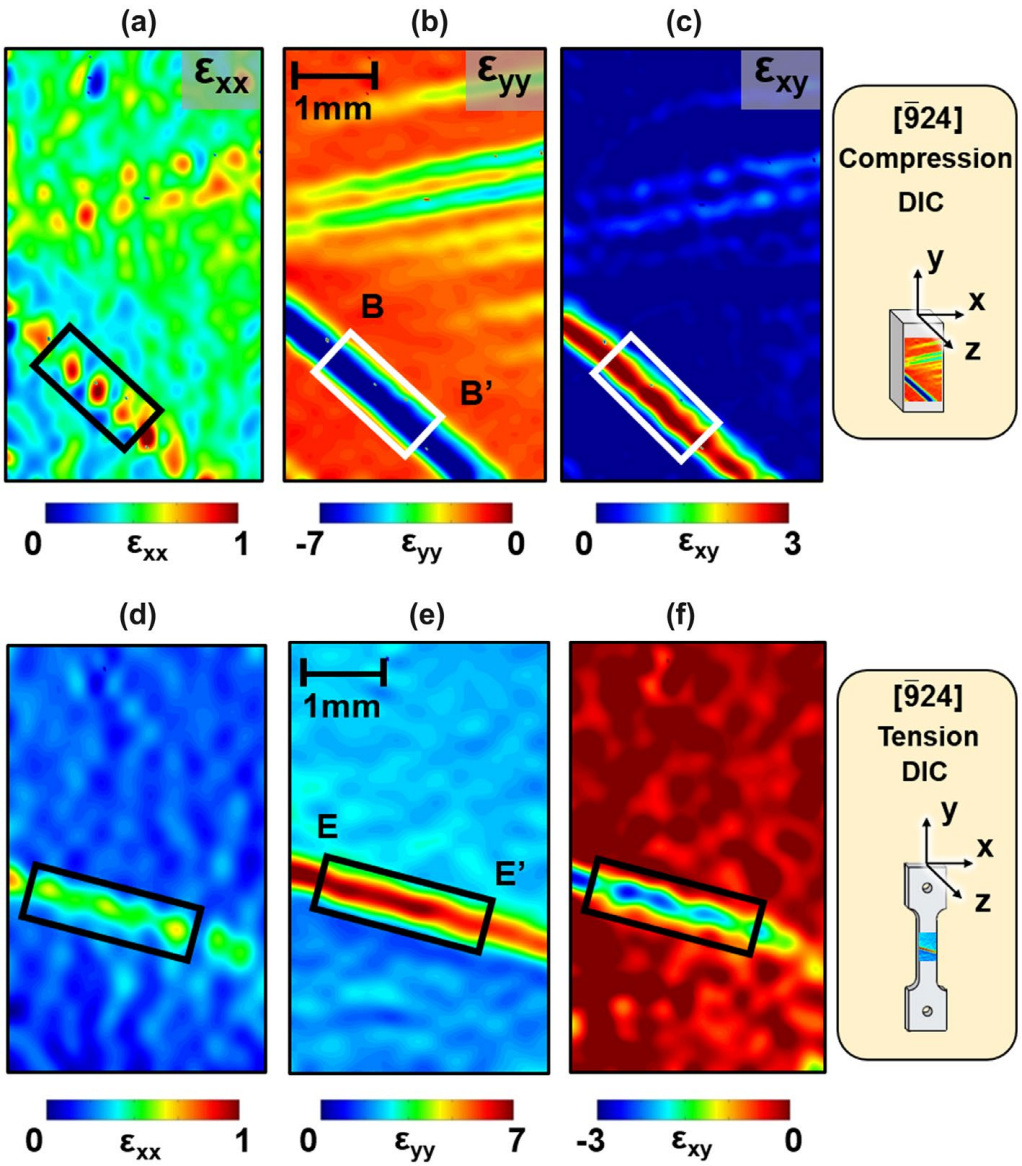

Figure 5. Three strain components (ε_{xx}, ε_{yy}, and ε_{xy}) produced by the slip shear on ($\bar{1}$ 1 0) plane (BB′ and EE′) are shown for [$\bar{9}$ 2 4] case under both compressive and tensile loading states. The local strain values are extracted from the rectangular region (2 mm × 0.5 mm) illustrated on the DIC strain contours.

Table 2. Experimental measurements of strain tensor for [$\bar{9}$ 2 4] samples subjected to compression and tension, respectively. The ratio of the strain tensor components measured in experiments in comparison with those calculated based on ($\bar{1}$ 1 0)[0 0 1] and ($\bar{1}$ 1 0)[1 1 1] shear. The ratios remove the shear magnitude effect (which evolves with shear stress). The ratios between the calculated strain components based on the ($\bar{1}$ 1 0)[0 0 1] shear are in close correspondence to the experimental results measured via DIC (more results will be provided in Discussion).

	Compression			Tension		
Loading axis [$\bar{9}$ 2 4]	$\varepsilon_{xx}/\varepsilon_{yy}$	$\varepsilon_{xx}/\varepsilon_{xy}$	$\varepsilon_{xy}/\varepsilon_{yy}$	$\varepsilon_{xx}/\varepsilon_{yy}$	$\varepsilon_{xx}/\varepsilon_{xy}$	$\varepsilon_{xy}/\varepsilon_{yy}$
Experiment	−0.78	−0.11	0.065	0.04	−0.18	−0.26
Model ($\bar{1}$ 1 0)[0 0 1]	**−0.84**	**−0.1**	**0.062**	**0.03**	**−0.2**	**−0.28**
Model ($\bar{1}$ 1 0)[1 1 $\bar{1}$]	−0.18	−0.43	0.43	0.42	−0.59	−0.36

Table 3. Experimental measurements of strain tensor for samples in $[\bar{1}\,0\,1]$ and $[1\,1\,\bar{1}]$ orientations subjected to compression and tension, respectively. The model results are from crystal plasticity shear equation given above showing the activation of $(0\,1\,1)[1\,0\,0]$ system for $[\bar{1}\,0\,1]$ case and $(0\,1\,\bar{1})[1\,0\,0]$ system for $[1\,1\,\bar{1}]$ case.

	Compression			Tension		
Loading axis $[\bar{1}\,0\,1]$	$\varepsilon_{xx}/\varepsilon_{yy}$	$\varepsilon_{xx}/\varepsilon_{xy}$	$\varepsilon_{xy}/\varepsilon_{yy}$	$\varepsilon_{xx}/\varepsilon_{yy}$	$\varepsilon_{xx}/\varepsilon_{xy}$	$\varepsilon_{xy}/\varepsilon_{yy}$
Experiment	−0.63	0.12	−0.084	−0.53	0.62	−0.37
Model(0 1 1)[1 0 0]	**−0.61**	**0.1**	**−0.062**	**−0.58**	**0.67**	**−0.25**
Model $(0\,1\,1)[1\,1\,\bar{1}]$	−0.56	0.64	−0.36	−0.21	0.34	−0.14
Loading axis $[1\,1\,\bar{1}]$						
Experiment	−0.21	−0.52	0.41	−0.78	−0.11	0.085
Model$(0\,\bar{1}\,1)[1\,0\,0]$	**−0.23**	**−0.5**	**0.46**	**−0.84**	**−0.1**	**0.062**
Model$(0\,\bar{1}\,1)[1\,1\,1]$	−0.84	−0.65	0.56	−0.56	−0.64	0.36

theoretical strain field in the crystal frame based on crystallographic slip shear as shown in Equation (4) [39], where $\varepsilon_{ij}^{\text{slip}}$ is the strain tensor in the crystal frame, n is the slip normal, l is the slip direction (Burger's vector direction), and γ is the glide shear strain on the candidate slip system. It is worth emphasising that this expression relates crystallographic shear to the crystallographic strain tensor. Secondly, to transform this crystallographic strain tensor to the sample frame strain tensor, we utilise Equation (5), where Q_{ij} is the transformation tensor between crystallographic and sample frames (det $Q = 1$). The candidate microscopic slip systems in $[\bar{9}\,2\,4]$ case are $(\bar{1}\,1\,0)[0\,0\,1]$ and $(\bar{1}\,1\,0)[1\,1\,1]$ as shown in Table 2. Finally, the comparison of the strain tensor in the sample frame and the experimentally measured local strain tensors enables us to identify the active slip system. The results have been tabulated in Table 2 for $[\bar{9}\,2\,4]$ case. By presenting the strain component ratios (as opposed to absolute values), the results are invariant to the magnitude of shear. It is indisputable that in all cases, the $\langle 0\,0\,1\rangle$ is the preferred slip direction in NiTi compared to the $\langle 1\,1\,1\rangle$ because of the remarkable agreement between measured and calculated strain ratios for $\langle 0\,0\,1\rangle$ case. This finding does not totally rule out the possibility of $\langle 1\,1\,1\rangle$ slip possibly at very high stresses; however, it is not observed in our current experiments. In $[\bar{9}\,2\,4]$ orientation, the predominant slip system is $(\bar{1}\,1\,0)[0\,0\,1]$. The Schmid factors for the $[\bar{9}\,2\,4]$ loading case are 0.30 and 0.48 for the $(\bar{1}\,1\,0)[0\,0\,1]$ and $(\bar{1}\,1\,0)[1\,1\,1]$ slip, respectively. This result is particularly noteworthy as the system with lower Schmid factor governs. Clearly, the energetics (generalised stacking fault energy curves) are an important considerations as discussed earlier [40] favouring the $\langle 0\,0\,1\rangle$ direction. The CRSS for slip is determined as 250 MPa.

$$\varepsilon_{ij}^{\text{slip}} = \frac{1}{2}\left(n_i l_j + n_j l_i\right)\gamma \tag{4}$$

$$\varepsilon_{ij} = Q_{im}\varepsilon_{mn}^{\text{slip}} Q_{nj} \tag{5}$$

4. Discussion of results

The research on NiTi SMAs continues to be exciting because many of their unusual behaviours remain inexplicable. In this study, we address two issues that have remained somewhat perplexing: the reasons behind the high ductility of the B2-NiTi [41] and the specific slip systems that are activated. The high ductility is a result of both slip and twin deformations, with twinning on $\{1\,1\,4\}$ system, and the crystallographic slip along $\{0\,1\,1\}\langle 0\,0\,1\rangle$.

There has been considerable debate in the literature whether {1 1 4} or {1 1 2} twinning is activated in NiTi [29], we show that {1 1 2} twinning is not observed in NiTi. Atomistic simulations show that {1 1 4} twinning is complex, involving synchronous shear action on four planes and internal shuffles [29]. It is also energetically more favourable compared to the {1 1 2} twinning. The present study shows that localised strain traces coincide with the {1 1 4} and not the {1 1 2} planes.

There has been considerable deliberation in the literature on the origins of high ductility of NiTi. The {0 1 1} slip cannot provide sufficient number of independent slip systems. At a first glance this family includes the following: (0 1 1)[1 0 0], $(0\ 1\ \bar{1})[1\ 0\ 0]$, (1 0 1)[0 1 0], $(1\ 0\ \bar{1})[0\ 1\ 0]$, (1 1 0)[0 0 1], and $(1\ \bar{1}\ 0)[0\ 0\ 1]$, for a total of six 'physically possible' slip systems. Among these six, there are in fact only three independent slip systems because the strain states developed by three of the systems can be a linear combination of the other three. Also, if loading was applied along any of the cube axes such as in this study, the cube would not be able to deform (because resolved shear stress is zero for all the possible ⟨1 0 0⟩ directions), hence there cannot be 'five' independent slip systems. On the other hand, if NiTi undergoes {1 1 4} twinning such as in the ⟨0 0 1⟩ compression loading case in this study, there are sufficient number of independent systems. The twinning occurs at a higher stress than slip and this results in much higher stresses above M_d, for example, for the [0 1 0] case which can in fact be beneficial [13]. By utilising single crystals, we eliminated the role of grain boundary constraints and permitted a transition from crystal scale to macroscale without the need to deal with grain–grain interaction effects. Also the choice of [0 1 0] direction as loading axis under compression may impart beneficial properties as the slip in this case cannot occur and twinning develops at higher stress levels. The possibility of designing new SMAs should consider the achievement of high austenite twin stress to extend the transformation of NiTi to high temperatures which is an ongoing research topic.

Similar results are expected in aged NiTi alloys with precipitates; however, in this paper, we isolated the role of the matrix flow (single phase B2) by eliminating the contribution from the precipitates. Nevertheless, the activation of the twinning in favourable orientations near the [0 1 0] pole is expected also in NiTi with precipitates where high stresses for activation are expected. This is consistent with early findings [13].

Since the CRSSs for {0 1 1} slip and {1 1 4} twin are determined as 250 and 330 MPa, respectively, we note that simultaneous activation of {0 1 1} slip and {1 1 4} twinning is a possibility depending on the crystal orientation and the stress state. We note that {1 1 2} is unlikely to occur based on the non-matching of localised plastic deformation traces in this study. The {1 1 2} twinning can potentially be activated at much higher stress levels [29,42].

Another question is whether the {0 1 1}⟨0 0 1⟩ slip can be verified in other crystal orientations subjected to tension and compression? To answer this question we made a comparison of the strain tensor components at macroscale for two other loading orientations (for $[\bar{1}\ 0\ 1]$ and $[1\ 1\ \bar{1}]$) both in tension and compression (four additional stress states). The results are summarised in Table 3.

We present the experimentally measured strain ratios in comparison with those calculated using the candidate slip systems. The agreement between experiment and calculation using (0 1 1)[1 0 0] slip for $[\bar{1}\ 0\ 1]$ case and $(0\ \bar{1}\ 1)[1\ 0\ 0]$ slip for $[1\ 1\ \bar{1}]$ case is noteworthy. Note that the well-known techniques such as the invisibility criteria ($g{\cdot}b = 0$) [43] have been traditionally used for determination of the Burger's vector direction. This approach has served the community well; however, the present approach provides a powerful alternative

amenable to evaluation at the mesoscale. The Schmid factors for the $[\bar{1}\,0\,1]$ case are 0.35 and 0.4 for $(0\ 1\ 1)[1\ 0\ 0]$ and $(0\,1\,1)[1\,1\,\bar{1}]$, respectively. For the $[1\,1\,\bar{1}]$ loading case, the Schmid factors are 0.47 and 0.27 for $(0\,\bar{1}\,1)[1\,0\,0]$ and $(0\,\bar{1}\,1)[1\,1\,1]$, respectively. This result is particularly noteworthy as it shows that $[1\,1\,\bar{1}]$ orientation (which is the predominant orientation for textured wires in NiTi) is rather susceptible to plastic flow.

Recent studies on crystal plasticity formulations for NiTi [44,45] underscore the importance of utilising the correct CRSS levels for slip and twinning and the correct description of the activated systems. The remarkable characteristic of the NiTi alloys is that activation of twin and slip can engender high ductility levels that are unprecedented among B2 alloys.

5. Conclusions

This work supports the following conclusions:

(1) In single crystals of NiTi, twinning occurs in $\{1\ 1\ 4\}\langle 2\ 1\ 2\rangle$ system whilst slip develops in the $\{0\ 1\ 1\}\langle 0\ 0\ 1\rangle$ system. Whether twinning or slip is favoured depends on the sample orientation. Near the $[0\ 1\ 0]$ pole, twinning is activated. Slip is favoured in $[\bar{1}\,0\,1]$, $[1\,1\,\bar{1}]$, and $[\bar{9}\,2\,4]$ tensile/compressive orientations. Both the CRSS values (250 MPa for slip and 330 MPa for twinning, respectively) and the Schmid factors (depending on the orientation the sample) decide the twin versus slip mechanism.

(2) By comparing the strain fields produced by $\langle 0\ 0\ 1\rangle$ vs. $\langle 1\ 1\ 1\rangle$ direction on $\{0\ 1\ 1\}$ planes, we are able to conclude unequivocally that $\langle 0\ 0\ 1\rangle$ family slip directions are favoured. This result fits with atomistic simulations that show lower fault energetics in $\langle 0\ 0\ 1\rangle$ direction.

(3) The exceptional high ductility exhibited by NiTi (as an ordered alloy) can partially be explained by the presence of slip and twinning providing sufficient number of independently active systems that can satisfy the Mises yield criteria. This makes NiTi a very unique alloy among the intermetallics family.

Acknowledgements

The EBSD analysis was carried out in part in the Frederick Seitz Materials Research Laboratory Central Research Facilities, University of Illinois. The authors are grateful to Mr. Changgong Kim for his assistance with the EBSD analysis. The single crystals were grown by Prof. Yuriy Chumlyakov of Tomsk State University, Russia.

Disclosure statement

No potential conflict of interest was reported by the authors.

Funding

This work was supported partially by Nyquist Chair funds and by the National Science Foundation, DMREF grant # 1437106.

References

[1] S. Miyazaki, K. Otsuka and Y. Suzuki, Scr. Metall. 15 (1981) p.287.
[2] S. Miyazaki, T. Imai, Y. Igo and K. Otsuka, Metall. Trans. A 17 (1986) p.115.
[3] L. Delaey, J. Ortin and J. Van Humbeeck, Phase Transf. 87 (1987) p.60.
[4] B. Strnadel, S. Ohashi, H. Ohtsuka, T. Ishihara and S. Miyazaki, Mater. Sci. Eng. A A202 (1995) p.148.
[5] N.S. Surikova and Y.I. Chumlyakov, Phys. Metals Metall. 89 (2000) p.196.
[6] D.A. Miller and D.C. Lagoudas, Mater. Sci. Eng. A 308 (2001) p.161.
[7] R.F. Hamilton, H. Sehitoglu, Y. Chumlyakov and H.J. Maier, Acta Mater. 52 (2004) p.3383.
[8] T.W. Duerig, Mater. Sci. Eng. A 438–440 (2006) p.69.
[9] D.M. Norfleet, P.M. Sarosi, S. Manchiraju, M.F.X. Wagner, M.D. Uchic, P.M. Anderson and M.J. Mills, Acta Mater. 57 (2009) p.3549.
[10] T. Simon, A. Kröger, C. Somsen, A. Dlouhy and G. Eggeler, Acta Mater. 58 (2010) p.1850.
[11] A.R. Pelton, G.H. Huang, P. Moine and R. Sinclair, Mater. Sci. Eng. A 532 (2012) p.130.
[12] T. Ezaz, J. Wang, H. Sehitoglu and H.J. Maier, Acta Mater. 61 (2013) p.67.
[13] H. Sehitoglu, I. Karaman, R. Anderson, X. Zhang, K. Gall, H.J. Maier and Y. Chumlyakov, Acta Mater. 48 (2000) p.3311.
[14] K.N. Melton and O. Mercier, Acta Metall. 27 (1979) p.137.
[15] K. Gall, H. Sehitoglu, Y.I. Chumlyakov and L.V. Kireeva, Scr. Mater. 40 (1998) p.7.
[16] S.W. Robertson, A.R. Pelton and R.O. Ritchie, Int. Mater. Rev. 57 (2012) p.1.
[17] Y. Wu, A. Ojha, L. Patriarca and H. Sehitoglu, Shape Memory Superelasticity 1 (2015) p.18.
[18] G.J. Pataky, E. Ertekin and H. Sehitoglu, Acta Mater. 96 (2015) p.420.
[19] L. Mañosa and A. Planes, Adv. Mater. 29 (2016) p.1603607.
[20] O. Benafan, R.D. Noebe, S.A. Padula, A. Garg, B. Clausen, S. Vogel and R. Vaidyanathan, Int. J. Plasticity 51 (2013) p.103.
[21] P. Sedmák, P. Ittner, P. Pilch and C. Curfs, Acta Mater. 94 (2015) p.257.
[22] P. Chowdhury and H. Sehitoglu, Prog. Mater. Sci. 85 (2017) p.1.
[23] R. Delville, B. Malard, J. Pilch, P. Sittner and D. Schryvers, Int. J. Plasticity 27 (2011) p.282.
[24] E. Hornbogen, J. Mater. Sci. 34 (1999) p.599.
[25] G.B. Olson and M. Cohen, Scr. Metall. 9 (1975) p.1247.
[26] A.N. Tyumentsev, N.S. Surikova, I.Y. Litovchenko, Y.P. Pinzhin, A.D. Korotaev and O.V. Lysenko, Acta Mater. 52 (2004) p.2067.
[27] J.D. Cotton, M.J. Kaufman and R.D. Noebe, Scr. Metall. Mater. 25 (1991) p.2395.
[28] E. Goo, T. Duerig, K. Melton and R. Sinclair, Acta Metall. 33 (1985) p.1725.
[29] T. Ezaz, H. Sehitoglu and H.J. Maier, Acta Mater. 60 (2012) p.339.
[30] E. Goo and P. Kee Tai, Scr. Metall. 23 (1989), p.1053-6.
[31] Y. Liu and S. Galvin, Acta Mater. 45 (1997) p.4431.
[32] C.P. Frick, A.M. Ortega, J. Tyber, A.E.M. Maksound, H.J. Maier, Y. Liu and K. Gall, Mater. Sci. Eng. A 405 (2005) p.34.
[33] A.J.W. Johnson, R.F. Hamilton, H. Sehitoglu, G. Biallas, H.J. Maier, Y.I. Chumlyakov and H.S. Woo, Metall. Mater. Trans. A 36 (2005) p.919.
[34] H. Sehitoglu, J. Jun, X. Zhang, I. Karaman, Y. Chumlyakov, H.J. Maier and K. Gall, Acta Mater. 49 (2001) p.3609.
[35] T. Saburi, *TiNi – shape memory alloys*, in *Shape Memory Materials*, K. Otsuka and C.M. Wayman, eds., Cambridge University Press, Cambridge, 1998, p.49.
[36] H. Tong and C. Wayman, Acta Metall. 22 (1974) p.887.
[37] J. Hansen, J. Pospiech and K. Lücke, *Tables for Texture Analysis of Cubic Crystals*, Springer, Berlin-Heidelberg, 1978.
[38] H.-J. Bunge, *Texture Analysis in Materials Science: Mathematical Methods*, Elsevier, Berlin, 2013.
[39] J.R. Rice, J. Mech. Phys. Solids 19 (1971) p.433.
[40] T. Ezaz, M.D. Sangid and H. Sehitoglu, Philos. Mag. 91, p.1464.
[41] K. Otsuka and X. Ren, Intermetallics 7 (1999) p.511.
[42] I. Karaman, A.V. Kulkarni and Z.P. Luo, Philos. Mag. 85 (2005) p.1729.

[43] D.B. Williams and C.B. Carter, *The transmission electron microscope*, in *Transmission Electron Microscopy*, David B. Williams and C. Barry Carter eds., Springer, New York, NY, 1996, p.3.
[44] S. Manchiraju and P.M. Anderson, Int. J. Plasticity 26 (2010) p.1508.
[45] J.A. Moore, D. Frankel, R. Prasannavenkatesan, A.G. Domel, G.B. Olson and W.K. Liu, Int. J. Fatigue 91 (2016) p.183.